RESEARCH ARTICLE

3D bioprinting-based single liver tumor spheroid analysis for aflatoxin B1-induced drug-resistant cancer cell

Viet Phuong Cao, Sera Hong, and Joon Myong Song*

College of Pharmacy, Seoul National University, Seoul 08826, South Korea

Abstract

Aflatoxin B1, found in a variety of foods, is a mycotoxin known to cause cancer. Therefore, humans may be exposed to it through their daily diet. In this study, a three-dimensional (3D) tumor spheroid model was developed via 3D bioprinting to examine whether exposure of HepG2 liver tumor spheroids to aflatoxin B1 can increase the population of drug-resistant liver cancer cells in a single tumor spheroid. Two biomarkers, CD133 (prominin-1) and aldehyde dehydrogenase 1 (ALDH1), were used to identify drug-resistant cancer cells formed in the single liver tumor spheroids. The induction of drug-resistant cancer cells in the single tumor spheroids was examined through single spheroid imaging and fluorescence-activated cell sorting (FACS). The increase of drug-resistant cancer cells, which was caused by aflatoxin B1 in a dose-dependent manner, was quantitatively monitored at the single tumor spheroid level using both methods. 3D bioprinting-fabricated single liver tumor spheroid model successfully determined drug-resistant liver cancer cells caused by aflatoxin B1.

Keywords: 3D bioprinting; Single tumor spheroid imaging; Aflatoxin B1; Drug-resistant cancer cell

1. Introduction

Cancer stem cells (CSCs) are known to be responsible for tumors' resistance to chemotherapies and radiotherapies, which lead to cancer treatment failure and cancer recurrence. CSCs have recently emerged as one of the most common targets for novel innovations in cancer therapies[1-4]. The distinctive characteristics and unique phenotype of CSCs are acquired as a result of abnormality in many pathways[5,6], including STAT3, Wnt/TCF, or NF-κB. Besides, transcription factors such as KLF4, c-MYC, and NANOG are overexpressed in CSCs, leading to the ability of metastasis, tumorigenesis, cell proliferation, and self-renewal, respectively. Among these characteristics, drug resistance is one of the key features, the mechanism of which involves many approaches[7,8]. Common processes include enhanced ATP-binding cassette transporter (ABC transporter) activity, by which the cells are protected by chemotherapy agents like doxorubicin or methotrexate, and apoptosis prevention via Rho-ROCK pathway.

The stem-like characteristics of CSCs are preserved and displayed by an array of markers, which are abnormally expressed because of modification in gene regulations. For example, CD44, a common marker in many cancer types, has been proven to not

only enhance cell–substrate interaction and cell response to stress, but also increase the level of resistance against cancer therapies[3,9]. Because a certain set of markers uniquely appear in CSCs rather than normal cancer cells, these markers can be utilized to distinguish and isolate CSCs from the entire population of various cancer cell lines[10-13].

Aflatoxin B1 is a mycotoxin derived from *Aspergillus flavus* and *Aspergillus parasiticus*. It is widely known as a carcinogen, particularly for liver cancer, by inducing a mutation in *p53* gene. Its metabolite by cytochrome P450 enzyme, exo-aflatoxin B1-8,9-epoxide, can link with guanine and generate an adduct with DNA. The interference to normal DNA structure by the DNA adducts can inhibit the activity of tumor suppressor genes. As a result, cell growth is no longer properly controlled, and cancer is initiated[14]. Aflatoxin B1 has been found in a wide range of foods, such as corn[15], peanuts[16], and rice[17]. Therefore, it is likely that humans absorb aflatoxin B1 through their daily diet. Previously, the correlation between aflatoxin B1 and liver cancer pathogenesis (or CSC) has been mainly studied using two-dimensional (2D) cell culture model[18]. However, several drawbacks of 2D cell culture have been highlighted. For example, in 2D cell culture, Birgersdotter *et al.* indicated that there is a loss in cell polarity, a pivotal feature of tissue, as well as an alteration in gene expression[19]. Moreover, it failed to preserve the natural morphology of cells and represented a similarity in the accessibility of cells to media and drug solutions, as observed in *in vivo* studies. This explains the significant difference between the results of *in vitro* studies using 2D cell culture and *in vivo* studies; it also highlights the need to develop a model relevant to physiological conditions to simulate biological processes in the body.

In contrast, three-dimensional (3D) cell culture has been proven to effectively simulate physiological conditions, particularly the tumor microenvironment. As the 3D-cultured cancer cells grow into a spheroid structure, they maintain their natural shape while forming a tumor-like cluster with inner and outer layers wherein oxygen, nutrients, and drug gradients form, making them less accessible to cancer cells in the inner layers[20]. Additionally, by allowing cancer cells to grow in a gel-like structure, 3D cell culture also mimics extracellular matrix (ECM)[21]. Previous studies have stated the important role of ECM in tumor microenvironment (TME)[22], in which it is the major component of the TME and supports unique characteristics of CSCs, such as drug resistance[23,24] and tumorigenesis[25]. Unlike 2D cell culture, which obviously lacks ECM, 3D cell culture, where cells are grown in a 3D structure, has a potential to simulate key features of ECM[26]. Firstly, ECM, which is composed by various macromolecules like laminin, collagen, and proteoglycan[27], can be similarly created by a mixture of biocompatible and natural polysaccharide and protein. Moreover, ECM stiffness, which is critical for metastasis[28], can be mimicked by cross-linking nature-derived protein or polymer. Furthermore, the 3D spheroid culture system is highly biologically relevant to native *in vivo* states in that 3D spheroids have the vital characteristics such as natural cell shape, a heterogeneous interface with the surrounding medium, and similar gene and protein expressions with the natural *in vivo* cancers[29,30]. Therefore, the results obtained in 3D cell culture model have been observed to resemble *in vivo* context, which is reflected by aspects like higher cell viability[31,32], higher yield of extracellular vesicles[33], more active drug metabolism[34], or higher levels of stem-like properties and epithelial–mesenchymal transition (EMT) markers, such as NANOG, SOX2, CD44, and CD133[35], compared to 2D cell culture. To date, a number of 3D cell culture techniques have been developed, which can be classified into scaffold-based and scaffold-free approaches[36,37]. Meanwhile, 3D bioprinting has been widely used in energy harvesting[38-40], food industry[41], tissue engineering[42-44], and cell biology[45-51]. In the present study, a scaffold-based 3D bioprinting *in vitro* model was developed to quantitatively determine drug-resistant single cancer cells formed in HepG2 tumor spheroids following the exposure to aflatoxin B1. The HepG2 cancer cell-laden hydrogel consisting of alginate and gelatin was 3D-bioprinted such that single cancer cells grown into tumor spheroids were uniformly distributed in the hydrogel. By using 3D bioprinting, size and shape of the hydrogel could be precisely controlled, and the porous structure of hydrogel after crosslinking could serve as an artificial ECM, where nutrients and soluble factors could be stored. The hydrogel entrapping cancer cells is allocated into a consistent cross structure with similar amount by 3D bioprinting, which not only makes the development of *in vitro* model less labor-intensive, but also remarkably enhances reproducibility. Owing to these advantages, the proposed model is expected to mimic physiological conditions. The present model is based on the assumption that human liver cancer patients, who are not aware of the tumor in their bodies, may be exposed to the carcinogen aflatoxin B1 through their diet. Particularly, this approach is greatly significant because it quantitatively evaluates the extent to which drug-resistant CSCs, which are not easily killed by anticancer agents, can be formed in single tumor spheroids when exposed to the carcinogen aflatoxin B1.

2. Materials and methods

2.1. Cell culture

Liver cancer cell line HepG2 from Korea Cell line bank (No. 30022, Seoul, Korea) was employed for the experiment

by culturing it in Dulbecco's modified Eagle's medium (DMEM; Gibco, Grand Island, NY, USA) supplemented with 10% fetal bovine serum (FBS; Gibco) and 1% antibiotic-antimycotic (Gibco) at 37°C under 5% CO_2. To maintain cell growth, media exchange was conducted every 48 h after washing with phosphate-buffered saline (1× PBS, pH 7.2, Gendepot, USA). When subculture was needed, the cells were washed with 1× PBS before detachment with trypsin (TrypLE Express, Gibco, Denmark) for 5 min.

2.2. Material preparation for 3D bioprinting
To mimic the ECM in tumor microenvironment, gelatin and alginate were purchased and employed in the lyophilized powder form. They were dispersed into 1× PBS at concentrations of 10% and 4% (w/v), respectively. The mixtures were heated up to 80°C in 7 h; to obtain a homogenous gel, they were mixed every hour, before being kept at 37°C. Finally, approximately 2.5 million HepG2 cells, prepared in 0.5 mL of DMEM supplemented with 10% FBS and 1% antibiotic-antimycotic, were added and mixed gently with the gel, which could be immediately applied to cell 3D printing.

2.3. 3D printing of mini-well
The CAD program Rhino 6 was used to design 3D mini-well structure. Subsequently, the design was converted into stl files for application in the New Creator K V1.57.70 software. Once the file was uploaded and the 3D printer was connected to the software, the fabrication of the mini-well was initiated automatically. Briefly, thermoplastic polylactic acid (PLA) polymer was transformed into a semisolid form by heating to 210°C, which flowed through the nozzle as semisolid fiber with a size of 0.2 mm. By optimizing the filling density and printing speed at 75% and 10 mm/s, respectively, layer-by-layer printing was facilitated to form a mini-well that was 4 mm high and covered an area of 14×14 mm. Each mini-well dish included nine wells arranged in a 3 × 3 square. An individual well had a size of 3 × 3 mm.

2.4. 3D bioprinting of cell-laden hydrogel
The 3D bioprinting of HepG2 cells in the hydrogel was conducted using the same 3D bioprinter and computer software as in the previous step. In particular, the prepared mixture of hydrogel and cells was loaded into a 10-mL syringe and fixed in the dispenser of the 3D bioprinter. Another stl file encoding the specialized design for gel printing was uploaded to the computer. Once printing commander was activated, the printer automatically printed the cell-laden hydrogel with cross-shaped structures into all nine individual PLA wells obtained from the previous step. After the cell-laden hydrogel was completely printed into the wells, the hydrogel was crosslinked by a 160-mM aqueous calcium chloride solution for 10 min. The

3D-printed cells were maintained at 37°C and 5% CO_2, with nutrients provided by DMEM supplemented with 10% FBS and 1% antibiotic-antimycotic, which was exchanged every 24 h. Their growths were monitored under the bright-field function of fluorescence microscope (Olympus BX51, Japan), wherein the diameter measurement is possible.

2.5. Aflatoxin B1 treatment
Aflatoxin B1 was purchased as a 5-mg powder in a vial (Enzo, Farmingdale, NY, USA). It was dissolved in dimethyl sulfoxide (DMSO) to give the stock solution with a concentration of 0.5 mg/mL; subsequently, it was kept at −20°C. For the treatment on HepG2 tumor spheroids, this stock solution was diluted in serum-free DMEM to three concentrations of 1, 2.5, and 5 μM. After a 7-day period of tumor spheroids' growth, DMEM supplemented with 10% FBS and 1% antibiotic-antimycotic was discarded, and the gel structures were washed twice with 1× PBS. Subsequently, different plates were treated with different concentrations of aflatoxin B1, along with the control, which contained only serum-free DMEM. The carcinogen incubation was performed for 48 h under the condition of 37°C and 5% CO_2.

2.6. Immunostaining for the detection of surface marker on tumor spheroids
Two important markers are found in the HepG2 liver cancer cell line. One is CD133, or prominin-1, a transmembrane glycoprotein that has been widely used to sort out liver CSCs. The other is ALDH1, a cytosolic enzyme, which is responsible for intracellular retinoic acid formation[52]. Owing to their significant role, this study employed these two markers to isolate and identify CSCs from the spheroids. After exposure to aflatoxin B1 at four different concentrations, the tumor spheroids were washed three times with 1× PBS. Subsequently, fixation was conducted by adding 4% paraformaldehyde (PFA) at 4°C to the samples in 20 minutes, followed by three washes with PBS. In the next step, permeabilization and blocking were done by immersing the samples into a 1× PBS solution containing 0.2% Triton-X and 1% FBS for 15 min. Following this, the samples were stained for 1 h with Anti-Alexa fluor 594 CD133 and Anti-Alexa fluor 647 ALDH1 antibody solutions at a dilution rate of 1:200, and then washed thrice with 1× PBS. Finally, counter-staining was required, using Hoechst 33258 (Bloomington, MN 55431) at a dilution rate of 1:500 for 15 min, followed by washing thrice using PBS. The fluorescence imaging of tumor spheroids was performed using confocal microscope (TCS SP8, Leica, Wetzlar, Germany) and LASX software after washing thrice with 1× PBS. The obtained images were analyzed with Imaris software (Bitplane, Zurich, Switzerland), whereas the fluorescence intensity was measured by Metamorph software (Molecular Devices, San Jose, CA, USA).
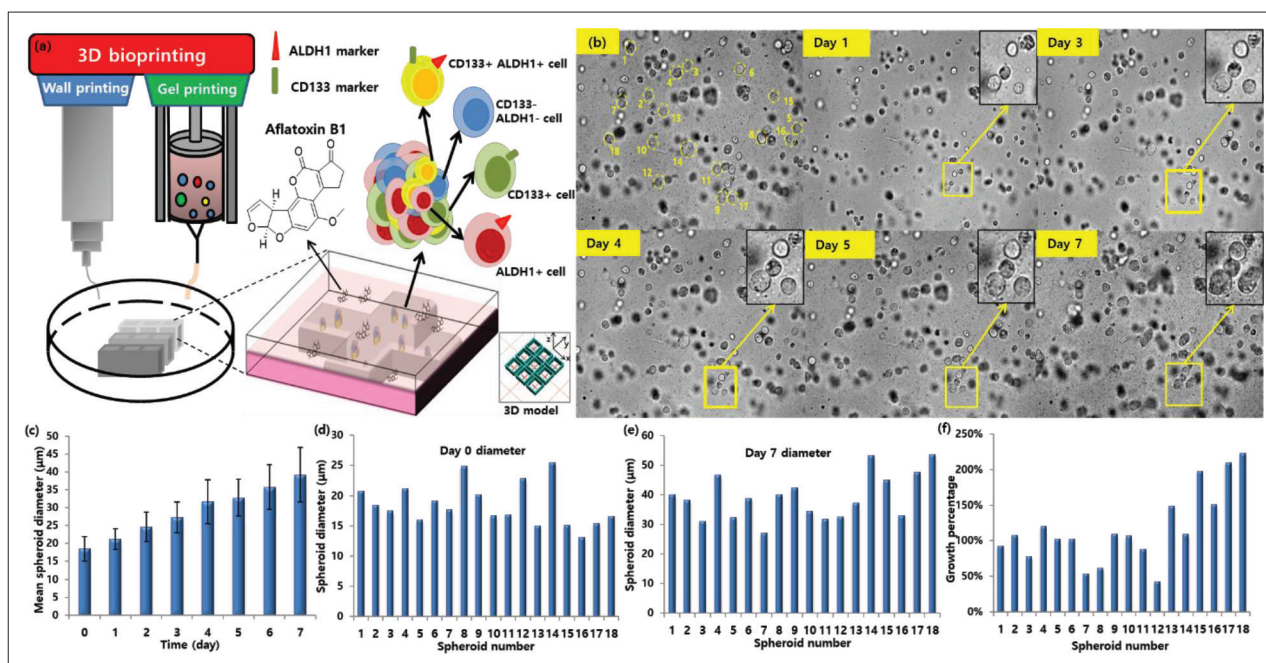
Figure 1. (a) Schematic diagram that depicts the formation of cancer spheroids and drug-resistant cancer cells via 3D bioprinting. Daily measurement of HepG2 liver tumor spheroids. (b) Numbered spheroids and bright-field images of the same region throughout a 7-day period. (c) Mean spheroid diameter throughout the period. (d) Diameters of spheroids measured on day 0 (immediately after printing). (e) Diameters of spheroids measured on the 7th day. (f) Growth percentage of all numbered spheroids.

2.7. Quantification analysis with fluorescence-activated cell sorting (FACS)

Initially, tumor spheroids were arranged randomly and maintained in the gel structure. To dissociate tumor spheroids from the hydrogel, 500 mg of collagenase NB 4G Proved Grade powder was dispersed in 5 mL double distilled water (DDW) to form a solution. Then, the collagenase solution was added to the hydrogel containing tumor spheroids. By incubating the hydrogel in the collagenase solution for 30 min at 37°C, the hydrogel structure was totally dissociated. The broken and dissolved hydrogels, along with the remaining spheroids, were collected and centrifuged at 1500 rpm for 1 min, and the supernatant was removed. The residue was dispersed in Accutase and incubated in 37°C; subsequently, the tumor spheroids were fully disintegrated into single cells. These single cells are fixed with 4% PFA at 4°C in 10 min. After fixation and discarding PFA, the single cells were washed twice by dispersing in PBS, centrifuging and discarding the supernatant. Subsequently, single cells were permeabilized and blocked with a mixture of 0.2% Triton-X and 1% FBS prepared in PBS for 10 min. In the next step, Anti-Alexa fluor 594 CD133 and Anti-Alexa fluor 647 ALDH1 antibodies were diluted in a PBS buffer containing 1% FBS, at a rate of 1:100, and applied to the single cells for 1 h. Finally, the antibody solution was discarded, and the single cells were washed with PBS. The single cells were then dispersed in buffer and applied to a BD flow cytometer for quantification analysis.

2.8. Statistical analysis

All the quantitative measurements were performed in three experimental replicates. The collected data are expressed as mean ± standard deviation (SD) from triplicate samples. A one-way ANOVA with Tukey's *post-hoc* test was performed to identify statistically significant differences.

3. Results

3.1. Development of tumor spheroids in hydrogel structure

To determine whether the bioprinting approach can facilitate proper spheroid formation, the diameters of the spheroids were measured over a 7-day period using the bright-field microscope. Spheroid images of the same position were taken every 24 h. Figure 1 shows the growth of spheroids and related measurement; an increase in the mean diameter of 18 different spheroids was observed (Figure 1c). The mean diameter started at an initial value of 18.5 μm and increased up to 39.2 μm on the 7th day, which corresponded to a relative growth of more than 210%. The growth rate was maintained quite steadily throughout the study period, despite a slight decrease from the 4th day to the 5th day. A fluctuation in growth of individual spheroids was clearly observed (Figure 1d and e). Eighteen different
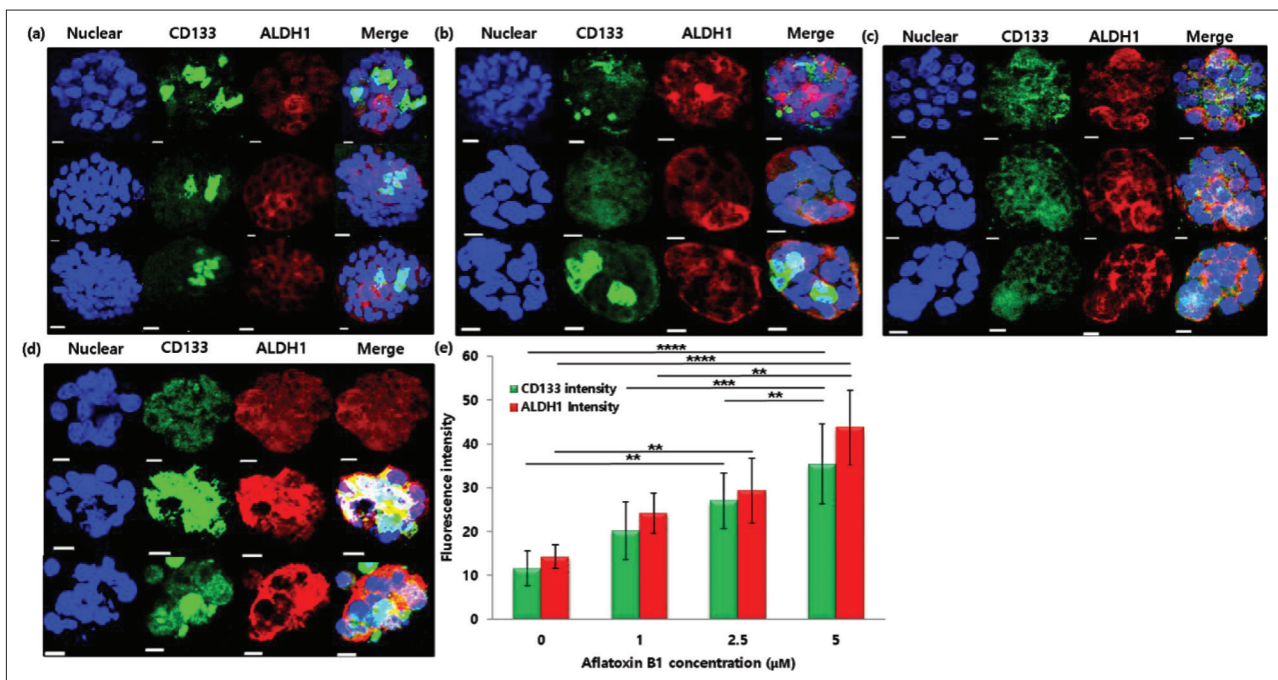
Figure 2. Confocal images of single tumor spheroids treated with aflatoxin B1 concentration of (a) 0, (b) 1, (c) 2.5, and (d) 5 µM. The expression of CD133 and ALDH1 was indicated by green and red colors, respectively, while the nucleus of single cancer cells was indicated by blue color. (e) Fluorescence intensities of CD133 and ALDH1 measured from the obtained images as a function of aflatoxin B1 concentration. All scale bars: 10 µm. $**P < 0.01$, $***P < 0.001$, $****P < 0.0001$.

spheroids showed different growth rate; spheroid number 18 grew up the most significantly by more than 220%, whereas the least growing spheroid, numbered 12, grew up by only 42% (Figure 1e). However, the difference in the size of spheroids was similar between the first day of 12.4 µm (from 13.1 to 25.5 µm) and 7th day of 16.6 µm (from 27.2 to 53.7 µm). This result suggests that the developed 3D bioprinting model is an appropriate platform for 3D tumor spheroid culture, which enabled the cells to grow naturally, thereby preserving the heterogeneity of the cell population. Moreover, as revealed in **Figure S1** in Supplementary File, the cell viabilities of tumor spheroids maintained more than 90% throughout the measurement period. These results demonstrated that the developed model could keep the cells alive without any special intervention.

3.2. Single tumor spheroids analysis based on the expression of cancer stem cell markers

Figure 2 shows the immunostaining results of HepG2 spheroids exposed to four different aflatoxin B1 concentrations, i.e., 0, 1, 2.5, and 5 µM, on the 7th day. The blue, green, and red signals indicate cell nuclei, CD133, and ALDH1 markers, respectively. The positivity of both CD133 and ALDH1 markers was partially shown in single cells of single HepG2 spheroids (Figure 2). The extents to which they were expressed increased as the concentration of treated aflatoxin B1 increased. CD133 is expressed on the HepG2 cell surface, while ALDH1 exists in the cytosol of HepG2 cells. Therefore, in HepG2 cells where both markers are found, an absolute overlap of these two markers cannot be detected. Instead, the fluorescence image of CD133 surrounds that of ALDH1. As revealed by the images of single spheroids, in the control, the fluorescence images of CD133 and ALDH1 were shown in a small region of the single spheroids, whereas the fluorescent images were expanded to a much larger region of the single spheroids at an aflatoxin B1 concentration of 5 µM. In detail, the average fluorescence intensities of two expressed markers were measured over the whole single spheroid surface. Table 1 displays the fluorescence intensity of the obtained images; both increased gradually from the control to the aflatoxin B1 concentration of 5 µM. In comparison to the control, wherein the average intensities of CD133 and ALDH1 were 11.6 and 14.5, respectively, the aflatoxin B1 concentration of 5 µM caused nearly three times increase in the average intensities of CD133 and ALDH1 (35.4 and 43.7, respectively) (Figure 2e). The increment in fluorescence intensities of CD133 and ALDH1 markers revealed that the drug-resistant properties of single HepG2 tumor spheroids were enhanced as a result of aflatoxin B1 treatment.

The number of single CSCs formed by exposure to aflatoxin B1 was determined at the single tumor

Table 1. Fluorescence intensity of the obtained images

| Group		CD133 intensity	Average	ALDH1 intensity	Average
Aflatoxin B1 0 μM	1	16.75	11.59	12.71	14.26
	2	10.36		14.98	
	3	8.09		9.81	
	4	10.99		18.43	
	5	15.92		16.08	
	6	7.46		13.55	
Aflatoxin B1 1 μM	1	10.74	20.13	23.43	24.16
	2	13.29		18.51	
	3	26.45		18.45	
	4	22.94		31.25	
	5	21.6		27.85	
	6	25.81		25.49	
Aflatoxin B1 2.5 μM	1	22.51	27.01	21.3	29.33
	2	17.58		22.79	
	3	27.22		21.87	
	4	27.74		35.06	
	5	31.53		36.51	
	6	35.53		38.5	
Aflatoxin B1 5 μM	1	19.03	35.38	28.96	43.70
	2	40.96		47.48	
	3	32.82		39.21	
	4	39.65		56.24	
	5	35.05		42.03	
	6	44.79		48.31	

spheroid level as a function of aflatoxin B1 using confocal microscopic imaging (Figure 3). Unlike above results (Figure 2), Figure 3 presents individual heterogenic response of single cancer cells in a single tumor spheroid to the carcinogen aflatoxin B1. The drug-resistant single cancer stem cell in the single spheroid was identified by the simultaneous expression of CD133 and ALDH1, which are shown in green and red, respectively. The yellow dots in the single spheroids corresponded to the single CSC. Each single cell in the single spheroids, denoted as gray dots, was identified by staining of their nuclei with Hoechst 33342. The total number of single cancer cells in a single spheroid was automatically calculated by a specific function of the IMARIS software that recognizes and counts the gray dots. The left images in Figure 3 show the total single cancer cells marked as gray dots in the single spheroids. The middle images in Figure 3 show CD133 and ALDH1 expressed in the single cells of left images. Considering the positivity of two markers, the right images present the drug-resistant single CSCs marked as yellow dots. The correlation between the formation of drug-resistant CSCs

and aflatoxin B1 treatment could be deduced by counting CSCs and determining their proportion over the total number of cancer cells in a single spheroid. The average CSC percentage in the single spheroids increased gradually when the aflatoxin B1 concentration increased (Figure 3e). It was determined to be 31% at aflatoxin B1 concentration of 5 μM, compared to 6.6% in the control. This result offers a clear insight into the effect of aflatoxin B1 on induction of drug-resistant CSCs at the single tumor spheroid level. Interestingly, the entire population of single cancer cells in single spheroids diminished as the concentration of aflatoxin B1 increased (Table 2).

3.3. Analysis of cancer stem cells via fluorescence-activated cell sorting

FACS analysis was employed as another method to examine the induction of drug-resistant single CSCs by aflatoxin B1 at the single spheroid level. FACS can detect single cancer cells isolated from single tumor spheroids fabricated via 3D bioprinting. After a 7-day period of growth, because cancer cells existed as spheroids where
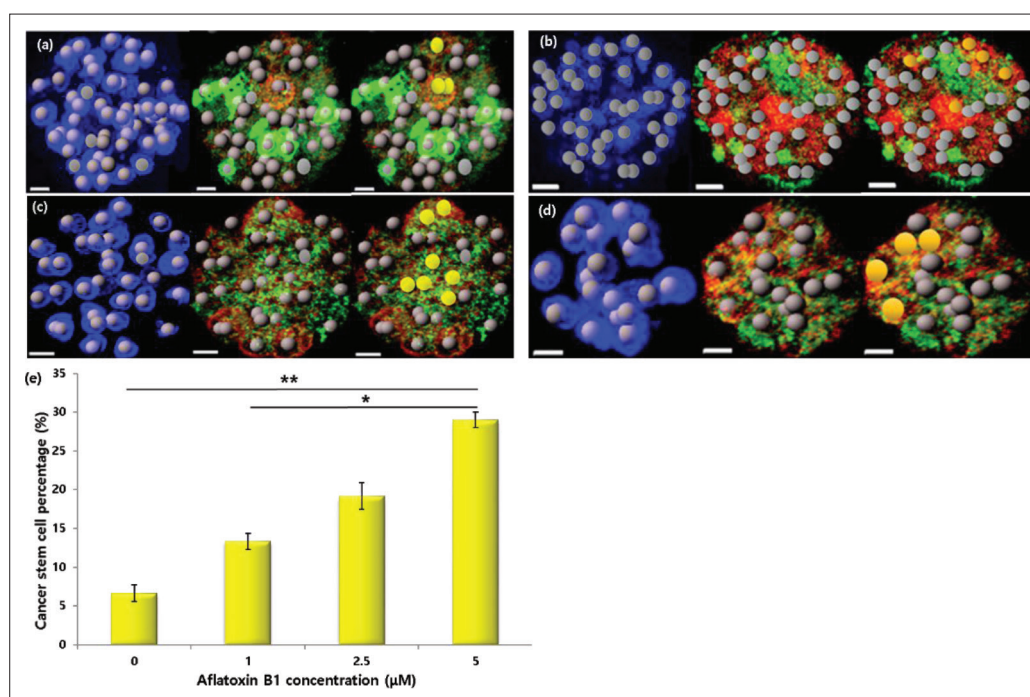
Figure 3. Representative images of spotted CSCs (indicated by yellow dots) and non-CSCs (indicated by gray dots) in single HepG2 spheroids treated with aflatoxin B1 concentrations of (a) 0, (b) 1, (c) 2.5, and (d) 5 μM. (e) Mean percentages of CSCs counted from obtained single spheroid images as a function of aflatoxin B1 concentration. All scale bars: 10 μm. *$P < 0.05$, **$P < 0.01$.

Table 2. Number of cells counted manually from acquired imaging data

Group		Total cells	CD133+ALDH1+ cells	%CSC	Average %CSC
Aflatoxin B1 0 μM	1	47	3	6.4%	6.63%
	2	53	3	5.7%	
	3	64	5	7.8%	
Aflatoxin B1 1 μM	1	41	5	12.2%	13.33%
	2	22	3	13.6%	
	3	28	4	14.2%	
Aflatoxin B1 2.5 μM	1	33	7	21.2%	19.19%
	2	27	5	18.5%	
	3	28	5	17.9%	
Aflatoxin B1 5 μM	1	18	4	22%	29%
	2	15	6	40%	
	3	17	4	23.5%	

cancer cells were attached to each other, collagenase NB 4G was utilized to disintegrate them into single cells so that flow cytometric analysis was possible. Figure 4 displays the result of FACS analysis for 10,000 single cancer cells disintegrated from HepG2 spheroids treated with the aforementioned concentration range of aflatoxin B1. In each graph, the horizontal and vertical axes indicate ALDH1 and CD133 emission, respectively. Based on the fluorescence intensities of ALDH1 and CD133,

single cancer cells were divided into four different types, corresponding to four quarters of the graphs. The upper-right quarter represented cancer cells positive for both CD133 and ALDH1, which signified CSCs defined by this study. As shown in upper-right quarter, the average CSC percentage in the entire isolated single cancer cells clearly increased as the concentration of aflatoxin B1 increased. At the control, CSCs accounted for approximately 6% of the whole population. As the concentration of aflatoxin
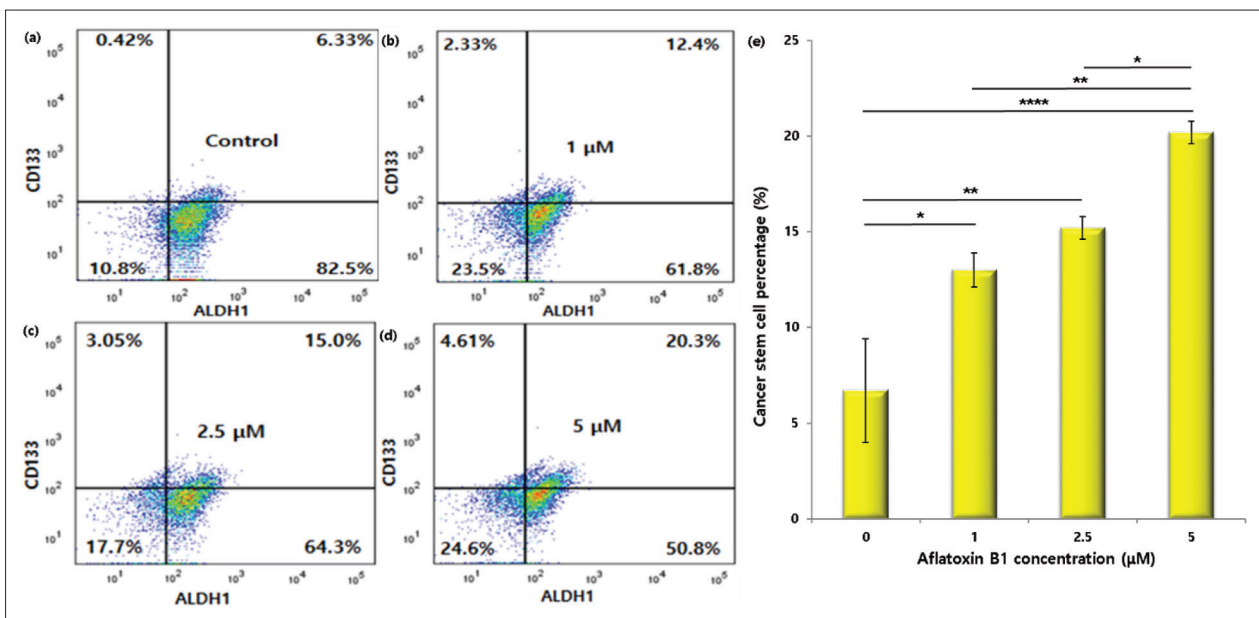
Figure 4. FACS analysis of CSCs isolated from HepG2 spheroids treated with aflatoxin B1 concentrations of (a) 0, (b) 1, (c) 2.5, and (d) 5 μM; (e) percentages of CSCs in HepG2 spheroids at four different aflatoxin B1 concentrations by FACS analysis. *$P < 0.05$, **$P < 0.01$, ****$P < 0.0001$.

B1 increased, the CSCs increased to 12.4% of the whole population at aflatoxin B1 of 1 μM, and further increased to 15% at aflatoxin B1 concentration of 2.5 μM. At aflatoxin B1 concentration of 5 μM, the number of CSCs increased to 20.3% of the total population. This result was consistent with the result obtained through confocal imaging of single spheroids.

4. Discussion

In 2020, liver cancer is estimated to account for 4.7% of the total new cancer cases globally, and it became the third most lethal cancer type, contributing to 8.9% of total deaths[53]. Moreover, the current therapeutic strategies for liver cancer have become more demanding due to resistance[54], and such problems have been mainly attributed to CSCs[55]. Regarding drug discovery, CSC is also one of the heated obstacles to new therapies[3]. Many toxins only target growing cancer cells and cell cycle, but their efficacies were not promising as expected since they are avoided by slowly dividing and dormant CSCs[1]. Meanwhile, CSC markers have been observed to exist on normal stem cells, human embryonic stem cells, or human tissues[5]. Antibody–drug conjugates (ADC) may be unable to distinguish targeted cells from healthy ones, leading to adverse effect and toxicity. Likewise, therapies targeting signaling pathways like Wnt, Notch, or Hedgehog also face similar challenges, since these cascades also progress in normal stem cells[2]. Moreover, approaches involving epigenetic processes and quiescent CSCs are limited due to a lack of knowledge about their function in CSC biology.

To date, CSCs have been defined by their clinical relevance and roles in cancer pathogenesis, rather than their biological characteristics[56]. Therefore, there is no fixed standard in terms of which surface markers must be expressed in CSCs, leading to differences in how various studies determined whether a cell population can be classified as CSCs or not. For example, Nguyen *et al.* utilized HepG2 cells and employed only the CD133 marker as the indicator for CSC isolation[57]. However, sorting CSCs using only one type of marker may not yield clinically significant result. In 2021, by reviewing the expression of CSCs marker in the literature, Dzobo *et al.*[1,58] revealed that the expression of only one individual marker was not considerably correlated with prognosis. In other words, classifying CSCs based on at least two markers should be recommended. In the present study, we selected CD133 and ALDH1 markers as the indication for sorting liver CSCs because of their significant roles in displaying CSC features[1]. While CD133 is involved a number of pathways related to drug resistance[59,60], ALDH1 is critical for oxidizing intracellular aldehydes[61] and facilitates cell proliferation[62]. The relative amount of approximately 6%, reflected by analysis using both confocal imaging and flow cytometry, suggests that this selection was appropriate to the proposed hypothesis of CSCs, which states that they are a rare population in tumors.

Aflatoxin B1 has been widely recognized as a carcinogen. Aflatoxin B1's metabolite, exo-aflatoxin B1-8,9-epoxide, can lead to various mutations in the p53 protein, among which the mutation at the third base codon 249 is

the most significant in cancer pathogenesis[63]. However, its role as a CSC inducer has not been thoroughly investigated. Kawasaki *et al.* isolated hepatoma K2 cells from rat exposed to aflatoxin B1[64]. They found that 89% of cell population was occupied by CSCs, while stemness genes such as *sox2*, *nanog*, and *klf4* were remarkably expressed. In addition, by treating HepG2 cells with various aflatoxin B1 concentrations and sorting out CSCs based on surface markers, Ju *et al.* confirmed a similar result regarding the ability of aflatoxin B1 ability to induce CSCs[18]. Nonetheless, both aforementioned findings were observed in 2D cell culture, which has been proven to have numerous limitations, making it clinically less significant. This study, which examines the phenomena in 3D tumor spheroid, may offer a novel and more remarkable insight into the actual effects of aflatoxin B1 on the formation of CSCs in a tumor.

In this study, two methods were employed to determine the presence of CSCs. Regarding single spheroid imaging, the analysis at the single-cell level indicated that the higher the aflatoxin B1 concentration for treatment, the lower the cell number in a spheroid. This could be attributed to the dual influence exerted by aflatoxin B1. Specifically, aflatoxin B1 not only induces CSCs but also causes DNA damage. This phenomenon is more evident at higher concentrations[65]. This could also explain the deviation between the results obtained from single spheroid imaging and FACS in the present study. In the results of single spheroid imaging and FACS, similarities could be observed in the control and low dose-treated samples. However, the difference in the number of CSCs acquired by FACS and imaging became more noticeable as the concentration of aflatoxin B1 increased. Indeed, as the tumor spheroids had a smaller number of single cancer cells, the percentage of single CSCs obtained by the spheroid imaging showed higher values of 19.2% and 29% at aflatoxin B1 concentrations of 2.5 and 5 μM, compared to 15% and 20.3%, respectively, acquired by FACS analysis at identical aflatoxin B1 concentrations. This is attributed to the growth of single tumor spheroids being significantly inhibited by the DNA-damaging aflatoxin B1, and this phenomenon occurs more frequently at higher concentrations of aflatoxin B1. As a result, Table 2 shows that there was smaller population of single cancer cells in single spheroids at higher concentrations of aflatoxin B1. In addition, owing to the growth-inhibiting effect of aflatoxin B1, more single cancer cells fixed in the hydrogel were observed. They could not be distinguished and excluded through the FACS analysis, although they could contribute to the entire population, regardless of which markers they expressed. However, it was obvious that the increase in the number of drug-resistant CSCs as the aflatoxin B1 concentration increased showed an identical tendency in both spheroid imaging and FACS analysis. This similar

tendency proved that single tumor spheroid imaging, like the frequently used FACS analysis, could also be an effective method for investigating the correlation between liver CSCs and the carcinogen aflatoxin B1. Furthermore, it should be noticed that single tumor spheroids for imaging and FACS analysis were fabricated by 3D bioprinting. The present study clearly demonstrated the possibility of drug-resistant CSCs forming in a single liver tumor spheroid by exposure to aflatoxin B1 carcinogen. A single tumor spheroid can correspond to a human patient having liver tumor based on the fact that the patient may be exposed to aflatoxin B1 through daily diet.

5. Conclusion

In the present study, we developed a 3D tumor spheroid model fabricated via 3D bioprinting to monitor the formation of liver CSCs induced by aflatoxin B1. CSCs were observed using single tumor spheroid imaging and FACS analysis. After using both methods, a correlation between aflatoxin B1 dose and CSC level was observed: the higher the aflatoxin B1 concentration for treatment, the higher the number of CSCs could be detected. The similarity between the detailed results of two methods suggests the suitability of 3D bioprinting-based single tumor spheroid analysis for quantification of drug-resistant single liver CSCs induced by aflatoxin B1.

Conflict of interest

The authors declare no conflicts of interests.

Author contributions

Conceptualization: Joon Myong Song
Formal analysis: Viet Phuong Cao, Sera Hong
Investigation: Viet Phuong Cao
Supervision: Joon Myong Song
Writing – original draft: Viet Phuong Cao
Writing – review & editing: Viet Phuong Cao, Joon Myong Song, Sera Hong

All authors approved the final version of the manuscript.

Ethics approval and consent to participate

Not applicable.

Consent for publication

Not applicable.

Availability of data

Data will be made available from the corresponding author upon reasonable request.

References

1. Dzobo K, Senthebane DA, Ganz C, *et al.*, 2020, Advances in therapeutic targeting of cancer stem cells within the tumor microenvironment: An updated review. *Cells,* 9(8): 1896.

2. Dzobo K, Senthebane DA, Rowe A, *et al.,* 2016, Cancer stem cell hypothesis for therapeutic innovation in clinical oncology? Taking the root out, not chopping the leaf. *Omics J Integr Biol,* 20: 681–691.

3. Batlle E, Clevers H, 2017, Cancer stem cells revisited. *Nat Med* 23**:** 1124–1134.

4. Ahn J, Choi HJ, Bang J, *et al.*, 2022, Ink-lithographic fabrication of silver-nanocrystal-based multiaxial strain gauge sensors through the coffee-ring effect for voice recognition applications. *Nano Converg,* 9: 46.

5. Walcher L, Kistenmacher AK, Suo H, *et al.*, 2020, Cancer stem cells-origins and biomarkers: perspectives for targeted personalized therapies. *Front Immunol,* 11: 1280.

6. Huang T, Song X, Xu D, *et al.*, 2020, Stem cell programs in cancer initiation, progression, and therapy resistance. *Theranostics,* 10(19): 8721–843.

7. Najafi M, Mortezaee K, Majidpoor J, 2019, Cancer stem cell (CSC) resistance drivers. *Life Sci,* 234: 116781.

8. Li Y, Wang Z, Ajani JA, *et al.*, 2021, Drug resistance and cancer stem cells. *Cell Commun Signal,* 19(1): 19.

9. Dzobo K, Sinkala M, 2021, Cancer stem cell marker CD44 plays multiple key roles in human cancers: Immune suppression/evasion, drug resistance, epithelial-mesenchymal transition, and metastasis. *Omics Journal of Integr Biol,* 25(5): 313–332

10. Fu JJ, Zhou Y, Shi XX, *et al.*, 2019, Spontaneous formation of tumor spheroid on a hydrophilic filter paper for cancer stem cell enrichment *Colloids Surf B: Biointerfaces,* 174: 426–434

11. Lapidot T, Sirard C, Vormoor J, *et al.*, 1994, A cell initiating human acute myeloid leukaemia after transplantation into SCID mice. *Nature,* 367(6464): 645–648.

12. Masciale V, Grisendi G, Banchelli F, *et al.*, 2019, Isolation and identification of cancer stem-like cells in adenocarcinoma and squamous cell carcinoma of the lung: A pilot study. *Front Oncol,* 9: 1394.

13. Suetsugu A, Nagaki M, Aoki H, *et al.*, 2006, Characterization of CD133+ hepatocellular carcinoma cells as cancer stem/progenitor cells *Biochem Biophys Res Commun,* 351(4): 820–824.

14. Verma RJ, 2004, Aflatoxin cause DNA damage. *Int J Hum Genet,* 4: 231–236.

15. Jayaratne WMSC, Abeyratne AHMAK, De Zoysa HKS, *et al.*, 2020, Detection and quantification of Aflatoxin B1 in corn and corn-grown soils in the district of Anuradhapura, Sri Lanka. *Heliyon,* 6(10): e05319.

16. Asl GB, Arvand M, Habibi MF, 2022, High affinity aptamers for ultra-sensitive detection of aflatoxin B1 in milk and groundnut samples with label-free photo-electrochemical aptasensor. *Food Chem,* 397: 133829.

17. Romero-Sánchez I, Ramírez-García L, Gracia-Lor E, *et al.*, 2022, Simultaneous determination of aflatoxins B1, B2, G1 and G2 in commercial rices using immunoaffinity column clean-up and HPLC-MS/MS. *Food Chem,* 395: 133611.

18. Ju H, Shim Y, Arumugam P, *et al.*, 2016, Crosstalk-eliminated quantitative determination of aflatoxin B1-induced hepatocellular cancer stem cells based on concurrent monitoring of CD133, CD44, and aldehyde dehydrogenase1. *Toxicol Lett,* 243: 31–39.

19. Birgersdotter A, Sandberg R, Ernberg I, 2005, Gene expression perturbation in vitro—A growing case for three-dimensional (3D) culture systems. *Semin Cancer Biol,* 15(5): 405–412.

20. Yip D, Cho CH, 2013, A multicellular 3D heterospheroid model of liver tumor and stromal cells in collagen gel for anti-cancer drug testing. *Biochem Biophys Res Commun,* 433(3): 327–332.

21. Antoni D, Burckel H, Josset E, *et al.*, 2015, Three-dimensional cell culture: A breakthrough in vivo. *Int J Mol Sci,* 16(3): 5517–5527.

22. Khalaf K, Hana D, Chou JT, *et al.*, 2021, Aspects of the tumor microenvironment involved in immune resistance and drug resistance. *Front Immunol,* 12: 656364.

23. Senthebane DA, Rowe A, Thomford NE, *et al.*, 2017, The role of tumor microenvironment in chemoresistance: to survive, keep your enemies closer. *Int J Mol Sci,* 18(7): 1586.

24. Senthebane DA, Jonker T, Rowe A, *et al.*, 2018, The role of tumor microenvironment in chemoresistance: 3D extracellular matrices as accomplices. *Int J Mol Sci,* 19(10): 2861.

25. Dzobo K, Senthebane DA, Dandara C, 2023, The tumor microenvironment in tumorigenesis and therapy resistance revisited. *Cancers (Basel),* 15(2): 376.

26. Dzobo K, Rowe A, Senthebane DA, *et al.* 2018, Three-dimensional organoids in cancer research: The search for the holy grail of preclinical cancer modeling. *Omics Journal Integr Biol,* 22(26): 733–748.

27. Dzobo K, Dandara C, 2023, The extracellular matrix: Its composition, function, remodeling, and role in tumorigenesis. *Biomimetics (Basel, Switzerland),* 8(2): 146.

28. Najafi M, Farhood B, Mortezaee K, 2019, Extracellular matrix (ECM) stiffness and degradation as cancer drivers. *J Cell Biochem,* 120(3): 2782–2790.

29. Ravi M, Paramesh V, Kaviya SR, *et al.,* 2015, 3D cell culture systems: Advantages and applications. *J Cell Physiol* 230(1): 16–26.

30. Jensen C, Teng Y, 2020, Is it time to start transitioning from 2D to 3D cell culture? *Front Mol Biosci*, 7: 33.

31. Bokhari M, Carnachan RJ, Cameron NR, *et al.,* 2007, Culture of HepG2 liver cells on three dimensional polystyrene scaffolds enhances cell structure and function during toxicological challenge. *J Anatom,* 211(4): 567–576.

32. Rodriguez-Salvador M, Fox-Miranda I, Perez-Benitez BE, *et al.*, 2022, Research dynamics of tissue spheroids as building blocks: A scientometric analysis. *Int J Bioprint,* 8(3): 585.

33. Kim JY, Rhim W-K, Cha S-G, *et al.*, 2022, Bolstering the secretion and bioactivities of umbilical cord MSC-derived extracellular vesicles with 3D culture and priming in chemically defined media. *Nano Converg,* 9(1): 57.

34. Schyschka L, Sánchez JJM, Wang Z, *et al.,* 2013, Hepatic 3D cultures but not 2D cultures preserve specific transporter activity for acetaminophen-induced hepatotoxicity. *Arch Toxicol,* 87(8): 1581–1593.

35. Huang YJ, Hsu SH, 2014, Acquisition of epithelial-mesenchymal transition and cancer stem-like phenotypes within chitosan-hyaluronan membrane-derived 3D tumor spheroids. *Biomaterials,* 35(38): 10070–10079.

36. Kawashima D, Yuki T, Li S, *et al.,* 2022, Non-invasive imaging of ion concentration distribution around cell spheroids by electrical impedance tomographic sensor printed on circuit board under temporal compensation by ion transport impedance model *Biosens Bioelectron,* 212: 114432.

37. Langhans SA, 2018, Three-dimensional in vitro cell culture models in drug discovery and drug repositioning, *Front Pharmacol,* 9: 6.

38. Ahmed A, Azam A, Wang Y, *et al.*, 2021, Additively manufactured nano-mechanical energy harvesting systems: Advancements, potential applications, challenges and future perspectives. *Nano Converg,* 8(1): 37.

39. Ranjan P, Gaur S, Yadav H, *et al.*, 2022, 2D materials: Increscent quantum flatland with immense potential for applications. *Nano Converg,* 9(1): 26.

40. Kim J, Lee J-K, Chae B, *et al.*, 2022, Near-field infrared nanoscopic study of EUV- and e-beam-exposed hydrogen silsesquioxane photoresist. *Nano Converg,* 9(1): 53.

41. Pérez B, Nykvist H, Brøgger AF, *et al.*, 2019, Impact of macronutrients printability and 3D-printer parameters on 3D-food printing: A review. *Food Chem,* 287: 249–257.

42. Samson AAS, Balwe SG, Hong S, *et al.*, 2023, Verification of nanomaterial-induced size-dependent human ether-à-go-go-related gene potassium channel blockage using three-dimensional bioengineered functional cardiac tissue constructs. *Chem Mater,* 35(2): 658–671.

43. Yu J, Lee S, Song J, *et al.*, 2022, Perfusable micro-vascularized 3D tissue array for high-throughput vascular phenotypic screening. *Nano Converg,* 9(1): 16.

44. Dong Z, Gong J, Zhang H, *et al.*, 2022, Preparation and characterization of 3D printed porous 45S5 bioglass bioceramic for bone tissue engineering application. *Int J Bioprint,* 8(4): 613.

45. Abdelrahim AA, Hong S, Song JM, 2022, Integrative in situ photodynamic therapy-induced cell death measurement of 3D-bioprinted MCF-7 tumor spheroids. *Anal Chem,* 94: 13936–13943.

46. Hong S, Song JM, 2021, A 3D cell printing-fabricated HepG2 liver spheroid model for high-content in situ quantification of drug-induced liver toxicity. *Biomater Sci,* 9(17): 5939–5950.

47. Hong S, Song JM, 2022, 3D bioprinted drug-resistant breast cancer spheroids for quantitative in situ evaluation of drug resistance. *Acta Biomater,* 138: 228–239.

48. Hong S, Song JM, 2023, High-resolution in situ high-content imaging of 3D-bioprinted single breast cancer spheroids for advanced quantification of benzo(a)pyrene carcinogen-induced breast cancer stem cells. *ACS Appl Mater Interfaces,* 15(9): 11416–11430.

49. Shao L, Hou R, Zhu Y, *et al.*, 2021, Pre-shear bioprinting of highly oriented porous hydrogel microfibers to construct anisotropic tissues. *Biomater Sci,* 9(20): 6763–6771.

50. Tetsuka H, Shin SR, 2020, Materials and technical innovations in 3D printing in biomedical applications. *J Mater Chem B,* 8(15): 2930–2950.

51. Wang T-Y, Li X-F, Liu S-M, *et al.*, 2022, Self-assembled wide bandgap nanocoatings enabled outstanding dielectric characteristics in the sandwich-like structure polymer composites. *Nano Converg,* 9(1): 55.

52. Clark DW, Palle KJA, 2016, Aldehyde dehydrogenases in cancer stem cells: Potential as therapeutic targets. *Ann Transl Med,* 4(24): 518.

53. Sung H, Ferlay J, Siegel RL, *et al.*, 2021, Global Cancer Statistics 2020: GLOBOCAN estimates of incidence and mortality worldwide for 36 cancers in 185 countries. *CA: Cancer J Clin,* 71(3): 209–249.

54. Miao Y, Yang T, Yang S, *et al.*, 2022, Protein nanoparticles directed cancer imaging and therapy. *Nano Converg,* 9(1): 2.

55. Zhou H-M, Zhang J-G, Zhang X, *et al.*, 2021, Targeting cancer stem cells for reversing therapy resistance: Mechanism, signaling, and prospective agents. *Signal Transduct Target Ther,* 6(1): 62.

56. Yu Z, Pestell TG, Lisanti MP, *et al.*, 2012, Cancer stem cells. *Int J Biochem Cell Biol,* 44(12): 2144–2151.

57. Nguyen ST, Nguyen LS, Nguyen THP, *et al.*, 2020, Isolation of cancer stem-like cells from hepatocellular carcinoma cell line HepG2 by methods of magnetic-activated cell sorting, spheroid culture, and anti-tumor drug-resistant selection: A primary evaluation. *Prog Stem Cell*, 7(1-2): 279–289.

58. Dzobo K, Ganz C, Thomford NE, *et al.*, 2021, Cancer stem cell markers in relation to patient survival outcomes: Lessons for integrative diagnostics and next-generation anticancer drug development. *Omics J Integr Biol,* 25(2): 81–92.

59. Lu R, Zhao G, Yang Y, *et al.*, 2019, Inhibition of CD133 overcomes cisplatin resistance through inhibiting PI3K/AKT/mTOR signaling pathway and autophagy in CD133-positive gastric cancer cells. *Technol Cancer Res Treatment,* 18: 1533033819864311.

60. Zhou L, Sun Y, Ye G, *et al.*, 2022, Effects of CD133 expression on chemotherapy and drug sensitivity of adenoid cystic carcinoma. *Mol Med Rep,* 25(1): 18.

61. Hiroyuki T, Tomohiro K, Ayumi N, *et al.*, 2017, *Updates in Liver Cancer,* Mohamed AH (ed.), IntechOpen, Rijeka.

62. Wei Y, Li Y, Chen Y, *et al.*, 2022, ALDH1: A potential therapeutic target for cancer stem cells in solid tumors. *Front Oncol,* 12: 1026278.

63. Link T, Iwakuma T, 2017, Roles of p53 in extrinsic factor-induced liver carcinogenesis *Hepatoma Res,* 3(6): 95–104.

64. Kawasaki Y, Adachi N, Yamazaki T, *et al.*, 2007, Cancer stem cells in aflatoxin B1-induced rat hepatocellular carcinoma K2 cells. *JSM Mycotoxins,* 57: 87–93.

65. Feng W-H, Xue KS, Tang L, *et al.*, 2017, Aflatoxin B1-induced developmental and DNA damage in caenorhabditis elegans. *Toxins,* 9(1): 9.